A CFD and experimental study on cavitation in positive displacement pump: benefits and drawbacks of the "full" cavitation model

Aldo Iannetti [a,*], Matthew T. Stickland [a], William M. Dempster [a]

[a] *Department of Mechanical and aerospace engineering, University of Strathclyde, 75 Montrose Street, Glasgow G1 1XJ, United Kingdom*

*E-mail: aldo.iannetti@strath.ac.uk (Corresponding Author)

ABSTRACT: To fill the lack of literature in the numerical study of Positive Displacement (PD) pumps in cavitating condition, a comprehensive and transient Computational fluid Dynamics (CFD) model of a PD pump, simulating the cavitation arising during the suction stroke, was created. The "full" cavitation model was utilised to study its capability on PD pumps cavitation. A set of three plunger speeds were simulated. Using the highest plunger speed an assessment was made of the effect of 1.5, 3, 4.5 and 15 ppm of air mass fraction on pump performance and cavitation. An experimental test rig, replicating the CFD model, was designed and built in order to validate the numerical model and find its weaknesses. CFD modelled, in a consistent way, the fluid dynamics phenomena related to cavitation (chamber pressure approaching the vapour pressure, the vaporization/condensation and the pressure spike occurrence at the end of the suction stroke marking the end of cavitation). On the other hand the CFD pressure trends calculated appeared stretched along the time axis with respect to the experimental data and this highlighted issues in the multiphase and cavitation models: the vaporization/condensation rate calculated by CFD did not follow the real dynamics correctly because the non-condensable gas expansion was overestimated. This was seen when comparing the CFD/experiments where the simulated pressure drop gradient, at the beginning of the suction stroke and the pressure peaks as the valve closed, exhibited a delay in their occurrence. The simulation results were sensitive to the dissolved air mass fraction as the delay depended on the amount of air dissolved in the water. Although the influence of the air mass fraction was considered consistent, the 3 ppm CFD case was the closest to the experiment results whereas the analyst expected the 15 ppm case to be more accurate.

Keywords: Cavitation in PD pumps, air fraction and cavitation, experimental validation of cavitation CFD model, Full cavitation model.

Introduction

Positive Displacement (PD) pumps have been overlooked by most users for years even if they may offer significant opportunities to improve processes, efficiencies and reduce costs (Parker, 1994). Nowadays PD pumps are becoming essential in some technologies, such as hydraulic fracturing, where centrifugal pumps cannot replace them. The performance in terms of achievable maximum pressure and a mass flow rate independent from the pressure head makes PD pumps the most suitable device for this kind of activity (Tackett, Cripe, & Dyson, 2008). On the other hand the design of PD pumps has not changed significantly over the years and the needs of the end user in terms of performance increment (e.g. mass flow rate), is becoming important. This has lead the manufacturers to revise the design of PD pumps to make them compatible with the requirement for increased performance in head and flow rate and a longer operating life which characterize a competitive device on the market.

Increasing the mass flow rate often means accelerating the plunger by means of increasing the crankshaft angular speed. In many cases this leads to problems related to the decrement of the Net Positive Suction Head available (NPSHa) and the increment of the velocity flow through the inlet valve which may become unacceptably high and cause cavitation damage (Eisenberg, 1963) and also erosion in the situations where slurries are pumped. The damage caused by these two phenomena is usually restricted to the inlet valve which may quickly lose its sealing property in a manner similar to what Price (Price, Smith, & Tison, 1995) observed. This will affect the volumetric efficiency of the device forcing the end user to stop the process in order to replace the worn valves and valve seats. Decreasing cavitation and erosion under operating conditions leads to a longer life valve and money saving for the end user. Many authors in the past have studied PD pumps by means of analytic methods such as 1D lumped parameter models. Very few of them have used CFD and this results in a gap in

the literature that the author of this paper would like to fill. To date, in fact, no comprehensive CFD models, such as the one described in this paper, have been reported in the technical literature.

This paper discusses the validity of a numerical tool based on CFD which analysts may use to support designers in creating longer lasting valves and valve seats by reducing cavitation during the suction stoke of positive displacement pumps. The model simulates the transient behaviour of a PD pump working in cavitating conditions throughout the inlet stroke. It is realistic because it represents the real fluid dynamics of the pump. The main achievements can be summarised as follows:

1. *Self-actuated valves.* The inlet valve is not actuated by the user but it moves when the pressure field, calculated by the solver, generates a force sufficient to exceed the valve spring preload.
2. *Moving mesh.* The plunger displacement is simulated by means of cell layer creation. During the simulation the volume of the pump chamber increases. The valve also moves so that the space between the valve and the valve seat grows when the valve lifts off the seat and diminishes when the valve returns to the seat.
3. *Multiphase and cavitation model.* The mixture multiphase model was utilised to handle the interaction between the water and the vapour. The interphase change rate was calculated by the "full" cavitation model discussed in the next paragraph.
4. *Effect of the non-condensable gas.* The cavitation model accounts for the presence of non-condensable gas which interacts with the cavitation.

The capability of the CFD model is tested by means of experimental validation. The test rig is described as well as the experimental campaign. The test rig employed was fully consistent with the CFD model created and represented the same pumping system under the

same operating conditions.

Experimental test rig description

Figure 1 shows the layout of the test rig pumping system. Water, at ambient conditions, flowed from the water tank to the PD pump through a Venturi pipe which was equipped with two pressure sensors. These transducers provided the pump inlet pressure signal and also the mass flow rate as the pressure drop across the Venturi pipe is proportional to the mass flow rate according to the Bernoulli's effect. After flowing into the pump chamber, the water was pumped back to the water tank via the outlet pipe in a closed loop system. A pressure sensor acquired the outlet pressure close to the pump outlet flange. The water tank had an opening to the exterior to provide it with the ambient pressure during the tests. Two pressure sensors placed in the vicinity of the inlet and outlet pipe connections made sure that the oscillation of the pressure at inlet and outlet during the test was negligible. The inlet and outlet pipes were fitted with two ball valves which had the duty of isolating the water tank from the pump when it was necessary to drain the pump without draining the whole system. During the tests ball valves number 3 and 4 were always wide open whereas the drain ball valve 5 and 6 were always closed.

[Insert figure 1]

A high performance linear servomotor was chosen to drive the pump plunger which was aligned and coupled to the motor shaft. The motor was controlled by the software provided with the motor and a closed loop fully automatic system ensured that the displacement produced by the linear motor was the same as the one commanded by the driver software.

Apart from the pressure sensor specified in figure 1, two additional sensors were placed on the pump. These transducers (shown in figure 2) acquired the pressure within the pump chamber and in the valve-seat lift volume. These locations were identified as the most significant for defining the fluid dynamics phenomena occurring in the pump. In fact:

- The chamber pressure trend describes how effective the decompression is carried out by the plunger displacement. The slope of the pressure drop during the induction stroke provides evidence of how the air mass fraction dissolved in the water slows down the formation of vapour (Iannetti, Stickland, & Dempster, 2014b).

- The valve-seat pressure trend describes the interaction between the chamber and the inlet manifold pressure as it drives the dynamic pressure due to the high velocity which characterises the flow in between the valve and the seat. The valve-seat lift volume is the zone where flow cavitation is initiated (K. Opitz & Schlücker, 2010).

[Insert figure 2]

Figure 2 shows the section of the pump taken on the symmetry plane. The top detailed view shows the location of the chamber pressure sensor which was screwed in a threaded hole cut in the side closing cup of the pump external case. The tapping location was very close to the Top Dead Centre position of the plunger. The bottom detailed view shows that four holes were drilled in the valve seat (two visible in the section). An annular recess and a hole in the pump external case created a path between the valve-seat volume and the pressure sensor which is shown on the far left side of the bottom detailed view. A transparent inspection window is visible to the right of the bottom (suction) valve. A high speed camera was placed

in front of the inspection window to take pictures of the lifting valve and vapour bubbles.

Table 1. Pressure sensor characteristics summary

Pressure sensor	Range [bar]	Abs/Rel	Max non linearity [% Range]	Response time [ms]
Venturi Upstream	0-2.5	A	0.25	< 0.5
Venturi downstream	0-2.5	A	0.25	< 0.5
Chamber pressure	0-10	R	0.25	< 0.5
Valve-seat pressure	0-10	A	0.25	< 0.5
Pressure outlet	0-6	A	0.25	< 0.5
Tank inlet	0-0.25	R	0.25	< 0.5
Tank outlet	0-0.25	R	0.25	< 0.5

Table 1 shows the characteristics of the pressure sensors used during the tests. The signals from the transducers were acquired by a National Instruments Compact Rio data acquisition system. The acquired signals were processed via a real time National Instruments Labview programme. The acquisition frequency for all the signals was 1 kHz. Tap water was utilised to fill the tank. 15 ppm of air mass fraction content in the water can be assumed as the tank was at ambient conditions. However, the air content was not measured.

Each test was carried out twice in order for the high speed camera to record the motion of the inlet valve with a frame rate of 1000 and 500 frames per second. According to the

specifications of the camera utilised, in fact, the 500 fps sequence allowed a wider view of the valve whereas the 1000 fps sequence gave a much more detailed view of the phenomena occurring in the valve-seat gap. The 500 fps sequence was utilised to visualise the valve together with the flow downstream the valve while the 1000 fps sequence was utilised to see only the flow through the valve. The 1 kHz frames were also used to measure the valve lift by an in-house post processing programme which measured the valve lift by comparing the displacement of a reference mark from the initial frame (zero lift) to the mark's location on subsequent frames.

It has to be noted that the analyst did not manage to measure accurately the mass flow rate because the Venturi pipe pressure sensors were very sensitive to the pressure waves and electromagnetic interference. The author leaves the improvement of the mass flow acquisition for the future research discussed in this paper.

Experimental tests description

Different from real applications, where the plunger is usually driven by a rotational motor/engine and the displacement of the plunger is operated by a crankshaft (Miller, 1995). In this work the plunger motion was operated by means of a linear motor controlled by its software as shown by figure 3. Three tests at three different plunger speeds were carried out. In each test of figure 3 the displacement-time history was fixed by a piecewise polynomial function composed of:

(1) A constant acceleration part of 4, 5.5, 7 m/s^2 respectively for test number 1, 2 and 3.

(2) A constant velocity part of 0.8, 0.95, 1.1 m/s respectively for test number 1, 2 and 3.

(3) A constant deceleration part of 4, 5.5, 7 m/s^2 respectively for test number 1, 2 and 3.

[Insert figure 3]

The plunger stroke in all of the tests was 0.204 m. Figure 3 represents the suction stroke only as the delivery stroke, which is not discussed in this paper, was carried out slowly and only to reposition the plunger to the TDC position again for the following test. The acceleration and velocity were designed to achieve the incipient, partial and full cavitation regimes (Iannetti, Stickland, & Dempster, 2015; K. Opitz & Schlücker, 2010; Karsten Opitz, Schlücker, & Schade, 2011).

CFD model description

Geometry and mesh

The CFD model replicated exactly the design of the test rig, from the water tank to the pump chamber. The outlet valve and pipeline were not modelled as the CFD simulated the suction stroke only. The fluid volume was extracted from the solid part which was then decomposed, as per the pattern shown in figure 4, in order to allow the creation of a hybrid mesh and also to set the moving mesh in the zones affected by the volume change (growing displacement volume due to the plunger motion) and motion (valve lift). The displacement volume growth was simulated by means of hexahedral cell layer creation in the direction of the plunger top surface motion. The plunger displacement volume and the valve lift volume were simulated by means of cell layer creation while the top and bottom volumes enclosing the valve external surfaces rigidly translated at the same velocity in order to leave the external shape of the valve unchanged during the motion. Top and bottom disks were respectively squeezed and stretched in order to guarantee the mesh continuity across the valve (Iannetti, Stickland, & Dempster, 2014a).

[Insert figure 4]

A mesh sensitivity test was carried out to define the proper mesh spacing in order to obtain the most accurate results with the lowest overall number of elements thereby decreasing the

computational cost. Table 2 shows the overall quality and size of the three meshes tested. Table 3 shows more details of the kind of mesh and size utilised for each fluid volume listed in figure 4.

Table 2: Mesh sensitivity analysis, three mesh sizes were tested.

Mesh	Number of Cells	Average Skewness	Approx computational time
1	3	0.24	48
2	5	0.26	60
3	6	0.22	72

Table 3: Mesh 2 details summary.

Location (see figure 4)	Volume description	Mesh type	Size details min-max	Mesh motion
1	Valve-seat lift	Hexahedral	0.2-1	Expanding
2	Inlet valve	Wedge	1-3	Compressing
3	Inlet valve	Hexahedral	2-3	Expanding
4	Displacement	Hexahedral	2.5	Expanding
5	Pump chamber	Tetrahedral	2.5-5	Static
6	Valve internal	Tetrahedral	1-2.5	Translating
7	Inlet manifold	Tetrahedral	2-4	Static
8	Valve top	tetrahedral	1-2	Translating

Boundary conditions and valve motion UDF

A fixed gauge pressure of 0 Pa was utilised as the inlet boundary condition. The fixed displacement motions described by figure 3 (test 1, 2 and 3) were fed in the CFD solver by means of a User Defined Function (UDF) which was attached on the plunger top surface moving mesh model to drive the displacement volume change. The valve lift moving mesh was handled by a second UDF attached to the CFD solver. This second programme coupled the pressure forces, acting on the valve, calculated at the end of each time step with the valve lift. The algorithm also accounted for the valve spring force as the spring stiffness characteristic was introduced in the overall force balance. By means of a first order Eulerian method, the UDF (figure 6) integrated numerically the overall force acting on the valve. From

this force the valve acceleration velocity and displacement were calculated. The displacement was utilised by the valve lift moving mesh algorithm in order to prepare the new mesh for the following time step operations.

[Insert figure 6]

CFD sub-models utilised and solver settings

The k-epsilon turbulence model was used as it provided better convergence over the k-omega model. The Enhanced wall treatment was used to correct the standard wall function in cases where the y+ values lay beyond the optimum range for the k-epsilon model (ANSYS, 2011b).

The Mixture model (ANSYS, 2011a) was used for the multiphase model. It was preferred over the other models present in the commercial software used (ANSYS Fluent) because of the low computational cost required. To account for the interphase change due to cavitation, the "full" cavitation model (Singhal, Athavale, Huiying, & Yu, 2002) was switched on. As explained by its author, this cavitation model accounts for the effect of non-condensable gas fraction dissolved in the water in an explicit way within the second phase. The model makes use of the ideal gas law, the pressure calculated by the CFD solver and the air mass fraction input by the user in order to calculate the air volume fraction. Test 1 and 2 ran with 3 ppm (parts per million) of air mass fraction while the full cavitation test (test 3) also ran with 1.5, 4.5 and 15 ppm to investigate the influence of the mass fraction on cavitation. Dissolved air, in fact, comes out of solution due to the pressure drop and interferes with cavitation (Wood, Hart, & Ernesto, 1998). Table 4 summarizes the settings chosen which were not discussed in this paragraph.

Table 4. Solver settings summary

Solver		RANS, pressure based, transient
Models	**Multiphase**	Mixture model (ANSYS, 2011a)

		Phases	Water liquid	Primary phase
			Water vapour	Secondary phase
	Turbulence	*k*-ε Standard	Enhanced wall treatment	
	Cavitation	Singhal et al.	3 ppm air (test 1,2 and 3), 1.5 and 4.5 ppm (test3)	
Pressure-Velocity coupling		SIMPLE		
Spatial discretization		Momentum	Second order upwind	
		Vapour	First order upwind	
		Turbulent kinetic energy	Second order upwind	
		Turbulent dissipation rate	Second order upwind	
Transient formulation		First order implicit		
Under relaxation factors		Pressure	0.3	
		Momentum	0.7	
		Vapour	0.5	
		Turbulent kinetic energy	0.8	
		Turbulent dissipation rate	0.8	
Residuals		10^{-3} Absolute		
Time step		3.4×10^{-4} s (test 3), 3.9×10^{-4} s (test 2), 4.5×10^{-4} s (test 1),		
Max Iteration per time step		45		
UDFs		Valve dynamics (figure 6) Plunger displacement-time		

The commercial finite volume software ANSYS fluent 15 was used as RANS solver on an Intel® XEON® CPU E5-1650 v3 @ 3.5 GHz processor with 16GB RAM. Three days were needed for a single run to simulate the entire suction stroke.

CFD monitors

During the CFD simulation the models were set to monitor every time step and store the data of the following quantities:

(4) *Chamber pressure*. A monitor point close to the TDC position of the plunger was created.

(5) *Valve seat pressure*. This monitor returned the volume weighted average of the static pressure in the valve-seat lift volume after every time step.

(6) *Inlet pressure*. This is the static pressure downstream the Venturi pipe.

(7) *Mass flow rate.*

(8) *Inlet valve lift.*

The monitor locations in the CFD were set to the same location as the pressure sensors in the experimental rig to allow comparison with the experimental data.

It was also decided that the following monitors, which had no counterpart in the experimental test, were of interest for the analysis:

- *Valve-seat vapour volume fraction*. This is the valve-seat lift volume weighted average of the vapour fraction.
- *Valve-seat air volume fraction*. This is the valve-seat lift volume weighted average of the air fraction which gets out of the solution because of the low static pressure.

CFD-Experiments results comparison

Test 1 incipient cavitation

Test 1 was designed to achieve the incipient cavitation regime by means of low plunger velocity and acceleration. The CFD model was set with 3 ppm of air mass fraction. Figure 7 shows the trend of (a) chamber and (b) valve-seat static pressure. Figure (a) shows that the minimum pressure in the chamber stays sufficiently above the vapour pressure. Figure (b) shows that the valve-seat minimum pressure is always higher than the chamber pressure. This is evidence of incipient cavitation. In fact, a small amount of vapour generation cannot be excluded as the static pressure could approach the vapour pressure locally in zones of high velocity or turbulence. This is demonstrated by the frame sequence of figure 9 where a small

amount of vapour is detected as, in some frames, the valve is partially obscured by the vapour cloud generated in the vicinity of the exit edge of the valve main body. The slope of the pressure decrement calculated by CFD, in both figure 7 (a) and (b), are lower than their experimental counterpart although the trends are in good agreement in the first half of the suction stroke.

[Insert figure 7]

Pressure spikes affect the second half of the suction stroke. They are present in both the experiment and the CFD plots although the latter show a delay in the spike's occurrence. It would appear that the CFD pressure trends are stretched along the time axis when compared to the experiments plots.

[Insert figure 8]

As the CFD is affected by low pressure longer than the experiment the maximum valve lift achieved by CFD is higher than the experiment, as highlighted by Figure 8 (b), which also shows the delay of the maximum valve lift occurrence compatible with the delay in the occurrence of the pressure spikes shown in figure 7. Figure 8 (b) demonstrates that the pressure spikes are the results of the water hammer effect related to the valve closing as the spike's temporal location corresponds to the negative valve velocity location in the valve-lift trend in both CFD and experiment. Errors in estimating the valve dynamics, affect the estimation of the pressure peak temporal location. However, beside the delay, in this case the trends are in good agreement with each other.

[Insert figure 9]

Figure 8 (a) shows how CFD estimates the composition of the second phase volume fraction in the valve-lift volume. The maximum vapour fraction calculated was 14% and occurred

roughly in the middle of the suction stroke. The average results are very low as the vapour quickly returned to negligible values.

Test 2 partial cavitation

Test 2 was designed to achieve the partial cavitating conditions. The CFD model was set with 3 ppm of air mass fraction as previously simulated in test 1. Figure 10 (a) and (b) show that the static pressure in both the chamber and the valve-seat locations were closer to the vapour pressure for a longer time, in the first half of the suction stroke, than test 1. The CFD lines were again shifted with respect to the experiments but the trends were in good agreement with each other from a qualitative view. In this test, the CFD predicts the water hammer effect but the magnitude of the resulting pressure spikes was larger than test 1.

[Insert figure 10]

Also in this case, because the CFD's low pressure lasted longer than the experimental counterpart, it may be assumed that the pressure forces across the valve created the lift force for a longer period of time. This resulted in a bigger and delayed valve lift achieved by CFD as shown in figure 11 (b). Figure 11 (b) also revealed that the CFD pressure spike's magnitude was overestimated because of the behaviour of the valve lift trend. In fact, while returning to the seat, according to CFD, the valve reversed its motion once (0.27 s). The experimental trend results are much smoother. It is important to show that the pressure peaks occur a little after the valve reverses the motion and, in the author's opinion, the valve reverse motion is the actual cause of the pressure spikes.

[Insert figure 11]

The maximum vapour fraction in the valve-seat lift volume, estimated by CFD and revealed by figure 11 (a) for test 2, was 14% this was similar to test 1 but the maximum level was kept

for more than a third of the overall suction stroke duration. Figure 12 shows twelve frames, evenly separated, taken by the high speed camera. The vapour generation was demonstrated to be non-negligible as in two of the images the valve is completely obscured by the vapour cloud.

[Insert figure 12]

Test 3 Full cavitation

Test 3 was the highest plunger speed test designed to achieve the full cavitating condition as explained by Opitz (K. Opitz & Schlücker, 2010). In this case the CFD simulations were run three times with 1.5, 3, 4.5 and 15 ppm of air mass fraction to shed light on the sensitivity of the CFD solution to the air content in the water.

[Insert figure 13]

Figure 13 shows the trend of (a) chamber pressure and (b) valve-seat lift volume static pressure. Both cases highlight a flat and low pressure which affects the first half of the suction stroke. During the first part of the suction stroke the experimental line and the 1.5 ppm CFD lines are overlapped in figure 13 (b). The same lines are very close to each other in figure 13 (a). High magnitude pressure spikes affected the second half of the suction stroke. The water hammer effects, in the experimental case, produce lower magnitude pressure spikes with respect to the CFD lines. In this case the magnitude of the pressure peaks (experimental line of figure 13 (a) and (b)) was overestimated by the CFD because of the valve bounces which are visible in figure 15. The peak's magnitude is predicted by all of the CFD lines but the occurrence was affected by a delay as in test 1 and 2. Both figure 13 (a) and (b) explain that the delay was affected by the air mass fraction. The more the air mass fraction, the bigger the delay in the CFD pressure spike's occurrence. Furthermore, the higher the air mass fraction the farther to each other the pressure lines lay (i.e. 3, 4.5, 15 ppm

CFD lines of figure 13 (a) and (b)). The 1.5 ppm curve produced the closest fit to the experimental line whereas the 15 ppm line shows the biggest delay.

[Insert figure 14]

Figure 14 was obtained by the CFD analysis and shows the vapour volume fraction (a) and the air volume fraction (b) in the valve-seat lift volume. The figures show that the higher the air content the lower the vapour generation and this agrees with what was postulated by Iannetti (Iannetti et al., 2014b).

[Insert figure 15]

A similar correlation between the air content and the NPSHr which affects vapour cavitation was also observed by Ding studying centrifugal pumps (Ding, Visser, & Jiang, 2012).

As the air expansion, shown by figure 14 (b), reveals a second peak after it reaches the zero volume fraction value around 0.25 s it may be assumed that the valve bounces on and off the seat once before completely closing. This is confirmed by the valve lift trend of figure 14. The 3 and 4.5 ppm CFD simulations clearly show that the valve touches the seat after 0.3 s and then lifts off it before closing completely at the end (or a little after) of the suction stroke. The 1.5 ppm simulation does not follow exactly the same pattern as in this case the valve reversed the motion at 0.27 s before touching the seat. The 15 ppm curve does not show the same behaviour as, for this case, the valve closes approximately when the plunger motion comes to the end.

The valve lift experimental trend deserves further discussion. The sequence of images shown in figure 16 demonstrates the large amount of vapour generated. In four frames out of 12, in particular, the valve was not visible because of the significant amount of vapour bubbles which is clear evidence of full cavitation. In these frames the graphical post processing

programme, which estimated the valve lift, failed and caused the gap in the experimental valve lift data which may be seen in figure 15. However, the maximum valve lift can be estimated by interpolation and can be assessed to range between 3 and 3.5 mm which demonstrated that CFD, once again, overestimated the maximum valve lift. As discussed for test 1 and 2 the reason for the overestimation of the valve lift is the longer application of the lifting pressure force on the valve. Furthermore, until 0.1 s, the 1.5 ppm CFD simulation follows the experimental valve lift trend closely while the 15 ppm case is the least accurate even though 15 ppm was expected to be the real air content in the water utilised (tap water). The 3 and 4.5 ppm case lay consistently in between the 1.5 and the 15 ppm case.

[Insert figure 16]

[Insert figure 17]

Figure 17 shows the spectrum of the chamber pressure signals of figure 13a. From the figure the following remarks can be listed:

1. Besides the pumping frequency, the experimental line shows two high power frequencies which are not sufficiently damped. Above 10 Hz, the spectrum presents two more peaks which are barely visible (20 and 33 Hz). This means that, in the specific test case, the wave energy dissipation due to the turbulence is more effective above 15 Hz.
2. The 15 ppm results clearly show the behaviour of the system above the critical damping. This means that the multiphase CFD model damped the oscillations much more than in reality, highlighting issues in the physical properties of the mixture (water, air and vapour).
3. The 1.5 ppm results show non-damped high frequency components. Their presence can be explained by the fact that the turbulence model utilised was not capable of dampening correctly the high frequency components. Comparing these results with the 15 ppm data, it appears that the dampening in the CFD model is provided mainly by the action of the air rather than the main phase (water) which is not capable of providing the physical damping.

4. The 3 and 4.5 ppm CFD lines follow qualitatively the same trend of the 1.5 ppm line, showing damped components in the spectrum.

The FFT analysis suggests the analyst focus on the modelling and numerical issues associated with the effect of non-condensable gas on pressure wave prediction.

Highlights on the phenomena observed

According to the observations on the experimental and numerical data together with the discussion of the results in the previous paragraph, the following brief summary can be drawn:

- All the phenomena related to the fluid dynamics of cavitation were predicted by the CFD (the decompression, the interaction with the non-condensable gas, the vapour generation and the water hammer pressure peak which marks the end of cavitation). Increasing the plunger velocity the cavitation regime was worse as expected. Increasing the air content in the water: the vapour generated decreased. This proves the consistency of the model.
- CFD overestimates the valve maximum lift due to the overestimation of the low pressure duration. The reason for this is the failure of the cavitation model which accounts for the influence of the air mass fraction in cavitation. CFD overestimates the influence of the expansion of air on cavitation.
- CFD pressure lines are generally slightly above the experimental line in the low pressure region. CFD also overestimates the magnitude of the pressure spikes in figure 7, 10 and 13 as a consequence of the incorrect valve velocity trend prediction.
- Although the analyst expected to see a good match between the experiments and the 15 ppm CFD case, the 1.5 ppm CFD simulations were, in fact, the closest to the experimental trends.

The author identified the influence of the air expansion on the fluid dynamics of the pump in cavitating conditions. It should be investigated further as, in the opinion of the author, it is the main cause of the mismatch between the CFD and the experimental data.

It is clear that the explicit algorithm managing the volume fraction estimation and thus the influence of the air (discussed in the paragraph dedicated to the solver settings) did not work accurately. The numerical model overestimated the expansion of the non-condensable gas during the low pressure part (first half of the suction stroke). This affected the time the recompression (carried out at approximately constant pressure) needed to "eliminate" the air. This resulted in the longer application of the lifting force on the valve. Therefore, all the phenomena observed such as the overestimation of the valve maximum lift and the pressure peaks magnitude and frequency, should be considered a direct consequence rather than a further source of problems.

The reason why the air expansion in the mixture is not predicted correctly lies in the assumptions and the simplifications made by the cavitation model explained by Singhal (Singhal et al., 2002). Concerning the air mass fraction, the only effect accounted for by the model was the volume fraction which appeared and disappeared according to the pressure value in all the cells of the discrete model. The air volume fraction interacted with the pressure field only indirectly through the second phase volume fraction transport equation. No momentum equation of the air was solved either by the cavitation model or the multiphase mixture model. The energy involved in the air expansion is not present in the fluid dynamic field as the energy equation was not solved and the mixture momentum equation did not account for the exchange of momentum between the second phase and the primary phase. As a result the dynamics of the vapour bubbles was not taken into account, the bubbles expanded without any constraints and this justifies the 15 ppm CFD spectrum. Also the cavitation model does not account for the dynamics of the bubbles as the second

order terms of the Rayleigh-Plesset equation are neglected in the cavitation model utilised. Moreover there is another aspect the author would like to point out. During the experiments no measurement of the dissolved air content was carried out. However, the numerical model assumed the condensation of the entire mass of the dissolved gas. It would be interesting at this point to know whether or not fluid dynamic phenomena (for instance turbulence) can prevent part of the dissolved gas from coming out of the solution and taking part in the expansion of the second phase.

Conclusions and further improvements

An experimental test rig designed to test a PD pump in incipient, partial and full cavitating condition was designed and built to validate a CFD multiphase model which replicated exactly the test rig design and operating conditions. The multiphase model was equipped with the "full" cavitation model. The full cavitation CFD case was tested with 1.5, 3, 4.5 and 15 ppm of air mass fraction. The incipient and partial CFD simulations were run with air content in water of 3 ppm only. Measurements of chamber static pressure, valve-seat static pressure and valve lift were taken during the experiments and compared with the CFD counterparts. The analysis revealed good consistency as the CFD trends were in good qualitative agreement with the experiments. Given the significant complexity of the problem, the research also highlighted a reasonable accuracy which was affected by an unrealistic influence of the non-condensable gas expansion. The CFD demonstrated a smaller gradient of pressure drop at the beginning of the suction stroke and also a certain delay in the pressure spikes occurrence in the second part of the suction stroke when the water hammer effect, due to the valve closing, took place. The pressure drop gradient and the delay in the pressure spike occurrence depended on the air mass fraction; the lower the air content the lower the delay and the steeper the pressure gradient. CFD always overestimated the valve lift; the

CFD maximum lift was higher and shifted with respect to the experimental lift. The reason for the difference in predicting the lift was the longer application of the lifting pressure force on the valve estimated by CFD which, in turn, was caused by the slow recompression of the air with respect to the experiment. The main cause of the accuracy loss was found to be the failure of the algorithm within the cavitation model estimating the expansion/compression of the air and therefore its influence on cavitation. Further investigation on the applicability of the mixture model which was utilised (ANSYS, 2011a) should be carried out. Also, the air mass fraction, which was handled in an explicit way by the cavitation model, should be treated as a real third phase and solved via a dedicated transport equation in order to couple strongly the phases and account for the momentum exchange between phases. For future improvement the author suggests also that the real air content in the water utilised for the experiments should be measured.

An important key-parameter which could shed more light on the problem is the volumetric efficiency. This parameter, in fact, is directly related to the cavitation regimes as observed by Iannetti (Iannetti et al., 2015), the lower the volumetric efficiency the higher the integral of the vapour generated. Volumetric efficiency is very simple to calculate by CFD but very difficult to measure in an experimental rig. In the future, effort should be made to complete the experimental analysis and equip the rig with an accurate mass flow meter. Once the volumetric efficiency is accurately measured it can be compared with the CFD counterpart and help the analyst in isolating the numerical cause which leads to the issues observed and discussed in this paper.

REFERENCES

ANSYS. (2011a). ANSYS Fluent Theory Guide. ANSYS Inc.

ANSYS. (2011b). ANSYS FLUENT UDF Manual. ANSYS Inc.

Ding, H., Visser, F. C., & Jiang, Y. (2012). A practical approach to speed up NPSHR prediction of centrifugal pumps using CFD cavitation model. In *Proceedings of the ASME 2012 Fluids Engineering Summer Meeting.* Rio Grande, Puerto Rico, USA.

Eisenberg, P. (1963). *Cavitation Damage*. Office of Naval Research.

Iannetti, A., Stickland, M. T., & Dempster, W. M. (2014a). A computational fluid dynamics model to evaluate the inlet stroke performance of a positive displacement reciprocating plunger pump. *Proceedings of the Institution of Mechanical Engineers, Part A: Journal of Power and Energy*, *228*(5), 574–584.

Iannetti, A., Stickland, M. T., & Dempster, W. M. (2014b). An advanced CFD model to study the effect of non-condensable gas on cavitation in positive displacement pumps. In *11th international symposium on compressor & turbine flow systems theory & application areas SYMKOM 2014 IMP2*. Lodz, Poland.

Iannetti, A., Stickland, M. T., & Dempster, W. M. (2015). A CFD study on the mechanisms which cause cavitation in positive displacement reciprocating pumps. *Journal of Hydraulic Engineering*, *1*(1), 47–59.

Miller, J. E. (1995). *The reciprocating pump, theory design and use* (Second Edi). Krieger publishing company.

Opitz, K., & Schlücker, E. (2010). Detection of Cavitation Phenomena in Reciprocating Pumps using a High-Speed Camera. *Chemical Engineering & Technology*, *33*(10), 1610–1614.

Opitz, K., Schlücker, E., & Schade, O. (2011). Cavitation in reciprocating positive displacement pumps. In *Twenty-seventh international pump users symposium* (pp. 27–33). Houston, Texas.

Parker, D. B. (1994). Positive displacement pumps-performance and application. In *11th International Pump User Symposium*.

Price, S. M., Smith, D. R., & Tison, J. D. (1995). The effects of valve dynamics on reciprocating pump. In *Proceedings of the twelfth international pump users symposium* (pp. 221–230). Texas A&M University.

Singhal, A., Athavale, M., Huiying, L., & Yu, J. (2002). Mathematical basis and validation of the full cavitation model. *Journal of Fluids Engineering*, *124*(3), 617.

Tackett, H. H., Cripe, J. A., & Dyson, G. (2008). Positive displacement reciprocating pump fundamentals- power and direct acting types. In *Proceedings of the twenty-fourth international pump user symposium* (pp. 45–58). Texas A&M University.

Wood, D. W., Hart, R. J., & Ernesto, M. (1998). Application guidelines for pumping liquids that have large dissolved gas content. In *Proceedings of the 15th international pump user symposium* (pp. 91–98). Huston, TX, USA.

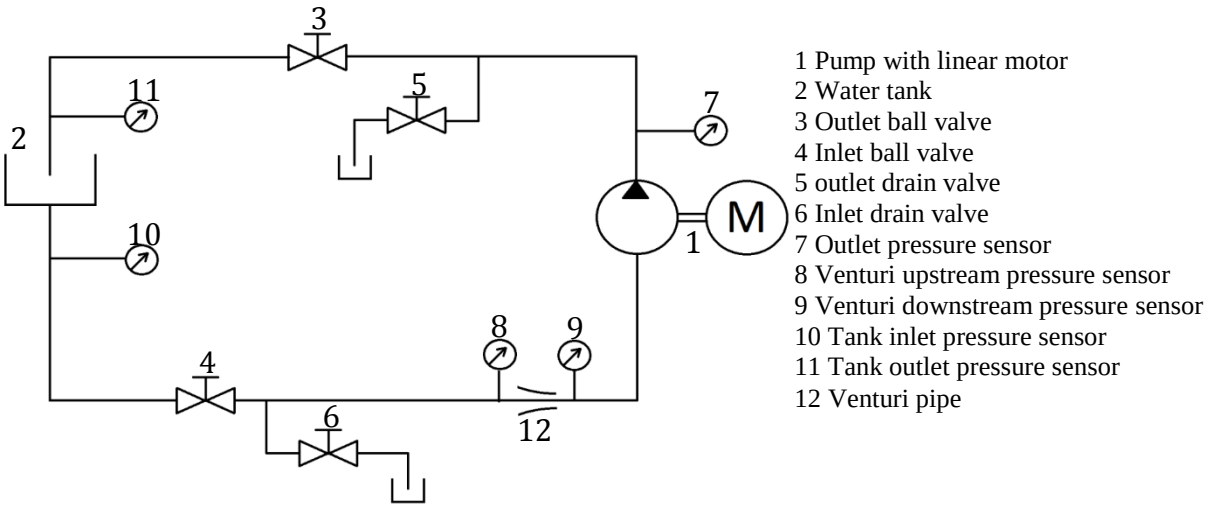

Figure 1: Test rig schematic with legend. The pumping system is shown, the pressure sensors on the pump are not shown.

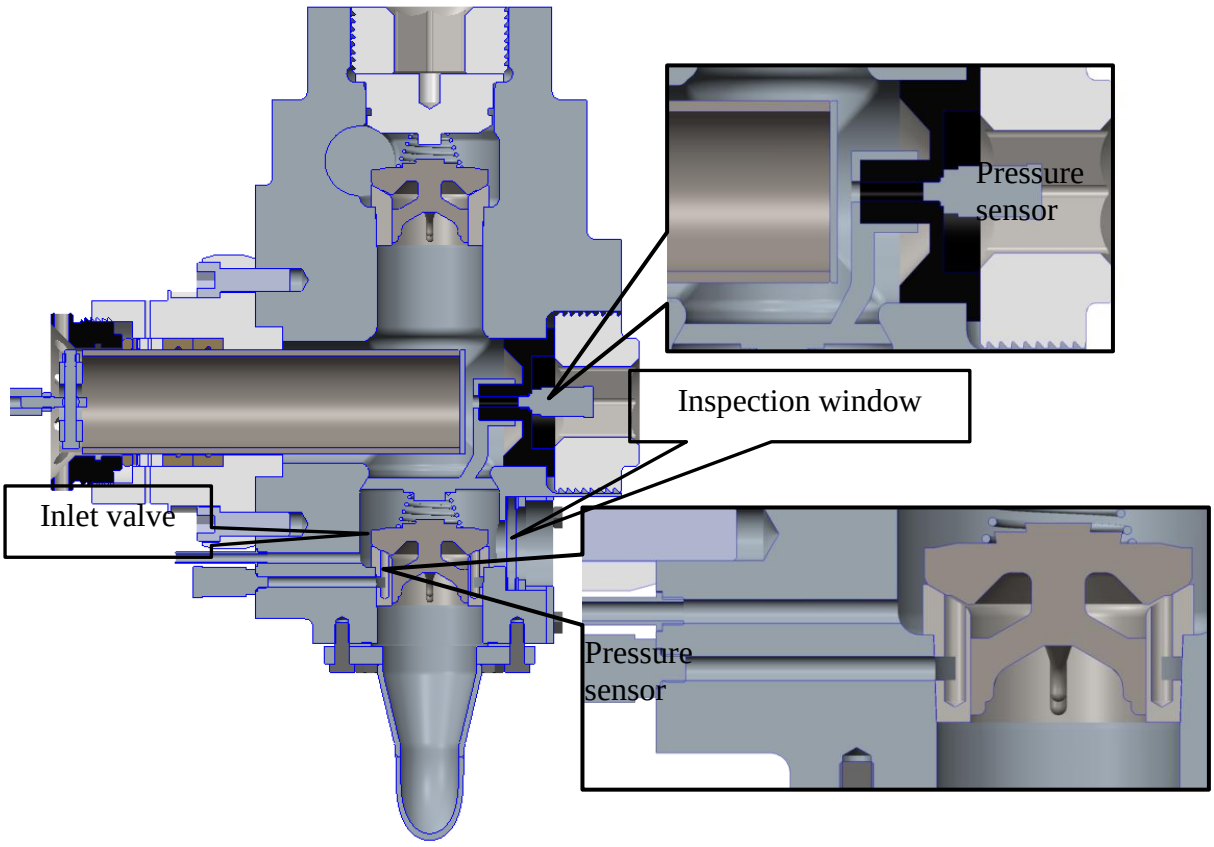

Figure 2: Section of the PD pump on the symmetry plane, the chamber and valve-seat pressure sensor locations are shown (respectively top and bottom detailed view), the inspection window on the right of the bottom (suction) valve is shown.

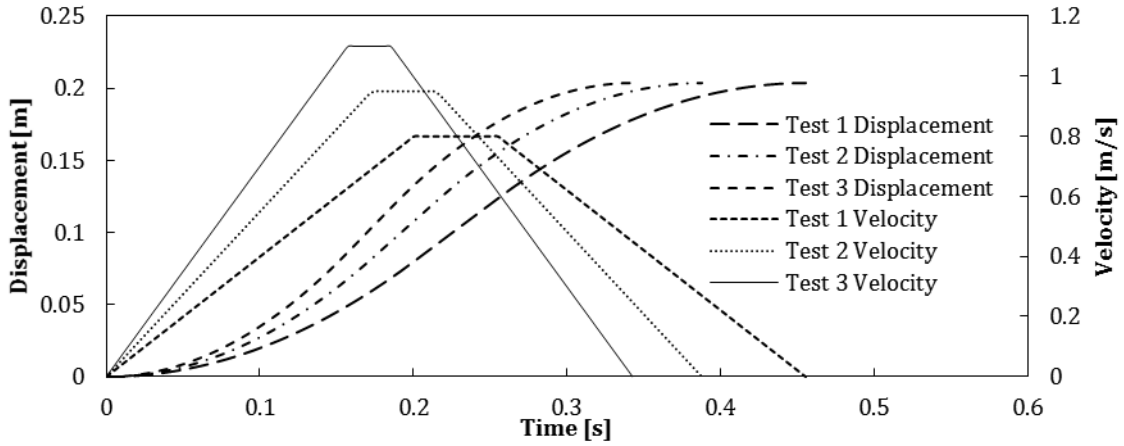

Figure 3: Plunger displacements and velocities fed into the motor drive administration software are shown.

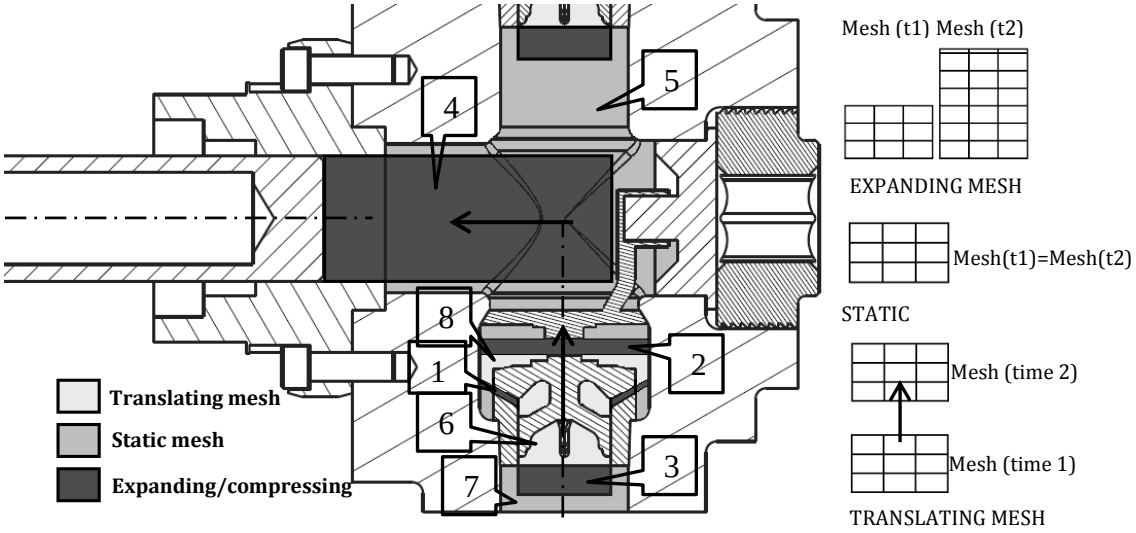

Figure 4: Decomposition pattern of the fluid volumes of the pump chamber (Iannetti, Stickland, & Dempster, 2014a), the numbered items are listed in table 3.

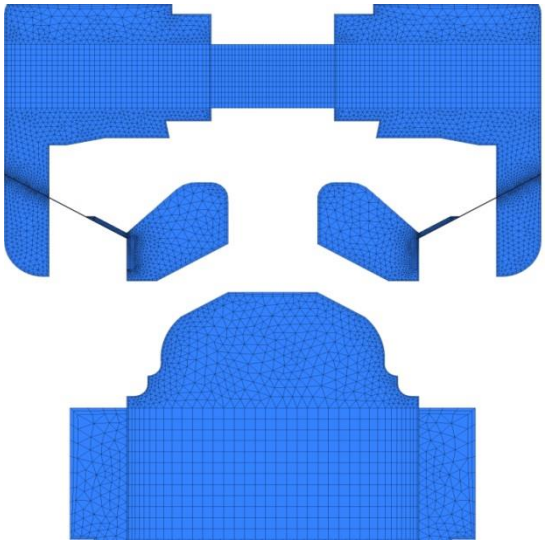

Figure 5: View of the mesh utilised for the analysis, detail of the mesh in the valve vicinity.

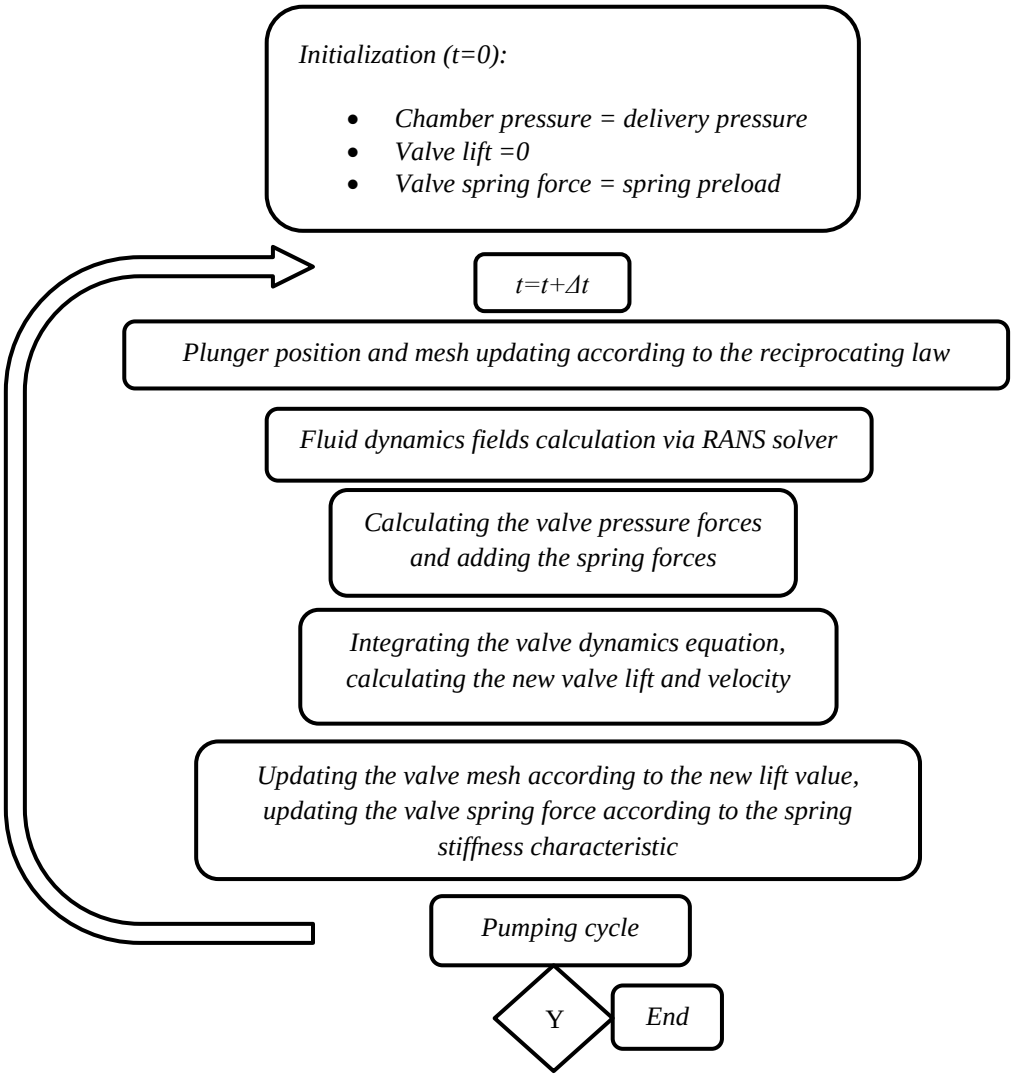

Figure 6: UDF scheme operations (Iannetti, Stickland, & Dempster, 2014b).

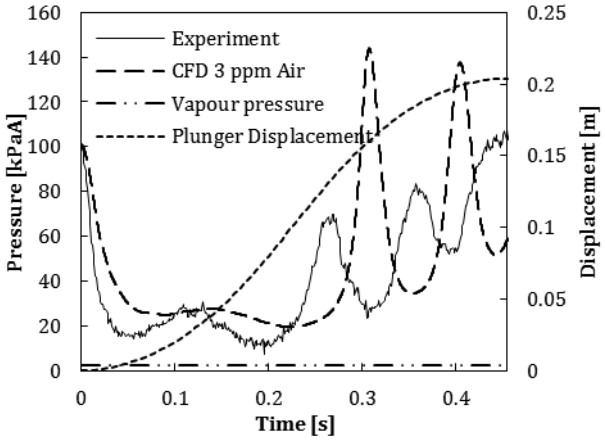

Figure 7a: Pump chamber static pressure. Experiments Vs CFD (test 1). CFD ran with 3 ppm air content in the water.

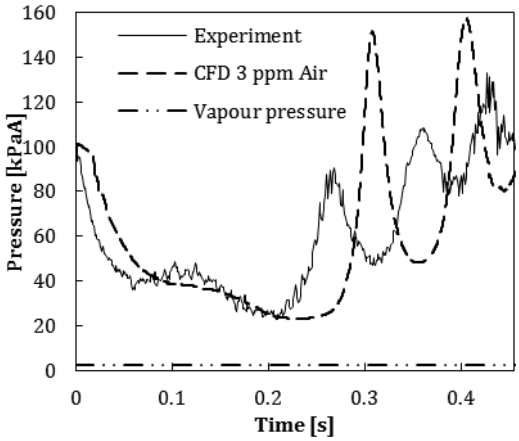

Figure 7b: Valve-seat static pressure. Experiments Vs CFD (test 1). CFD ran with 3 ppm air content in the water.

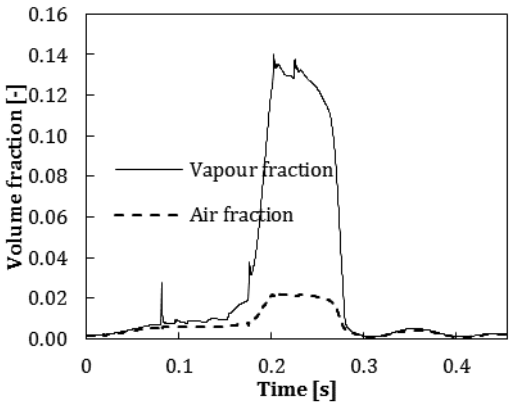

Figure 8a: Second phase fraction composition according to CFD (test 1).

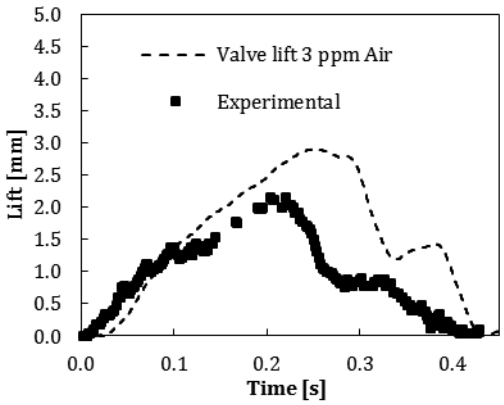

Figure 8b: Valve lift, Experiment Vs CFD (test 1). CFD ran with 3 ppm air content in the water.

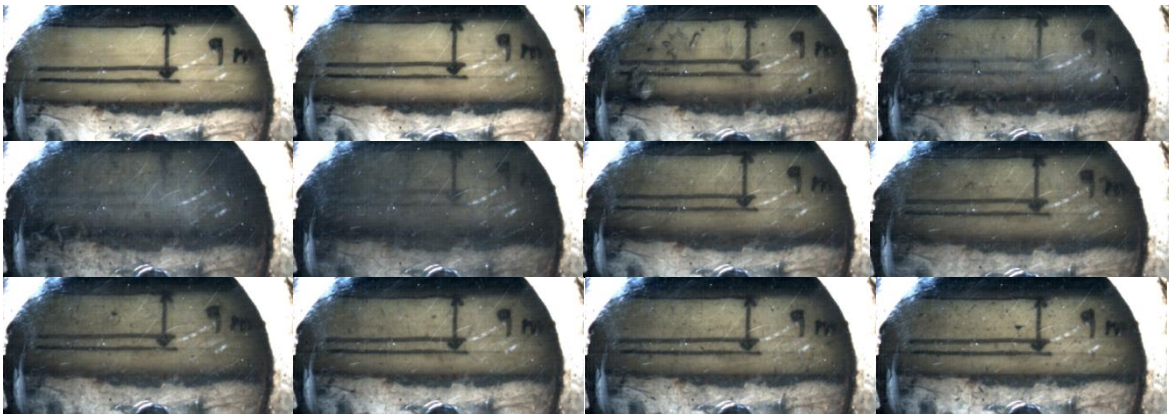

Figure 9: Null/incipient cavitation, only three frames show vapour which never obscure the view of the valve.

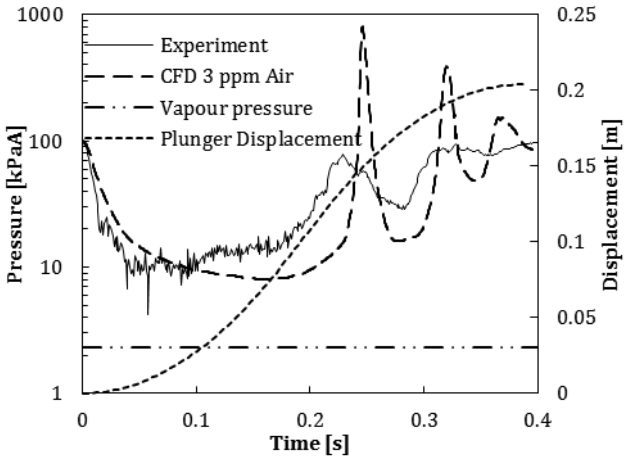

Figure 10a: Pump chamber static pressure (log scale). Experiments Vs CFD (test 2). CFD ran with 3 ppm air content in the water.

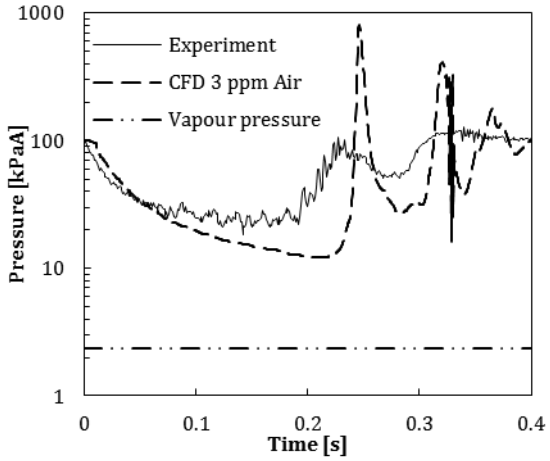

Figure 10b: Valve-seat static pressure (log scale). Experiments Vs CFD (test 2). CFD ran with 3 ppm air content in the water.

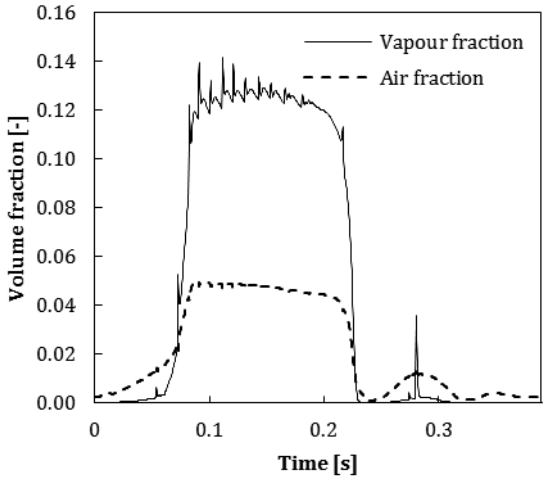

Figure 11a: Second phase fraction composition according to CFD (test 2). CFD ran with 3 ppm air content in the water.

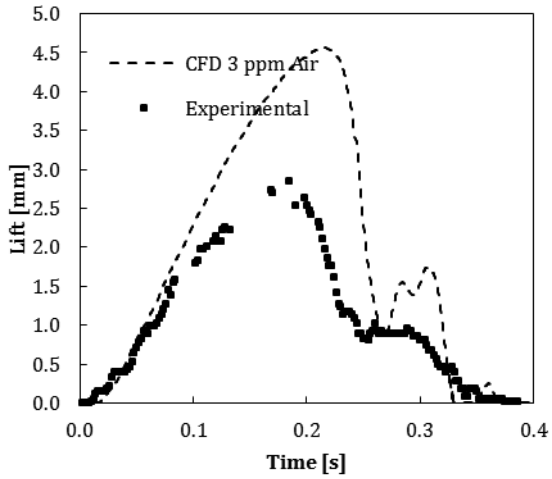

Figure 11b: Valve lift, Experiment Vs CFD (test 2). CFD ran with 3 ppm air content in the water.

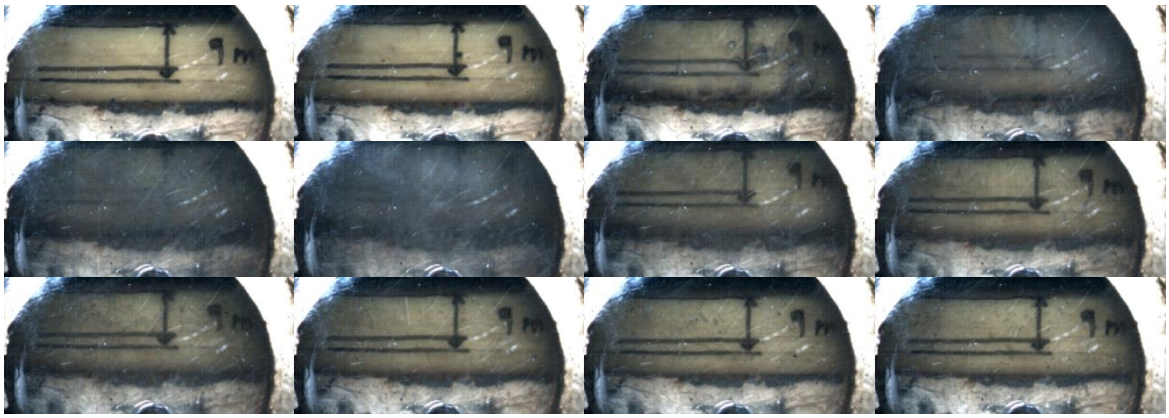

Figure 12: Partial cavitation. Four frames show a vapour cloud around the valve-lift gap, in two of them the view of the valve was obscured almost completely.

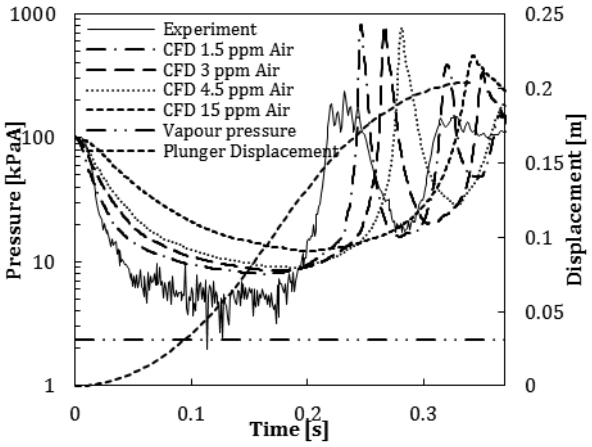

Figure 13a: Pump chamber static pressure. Experiments Vs CFD (test 3), the sensitivity to the air mass fraction is shown.

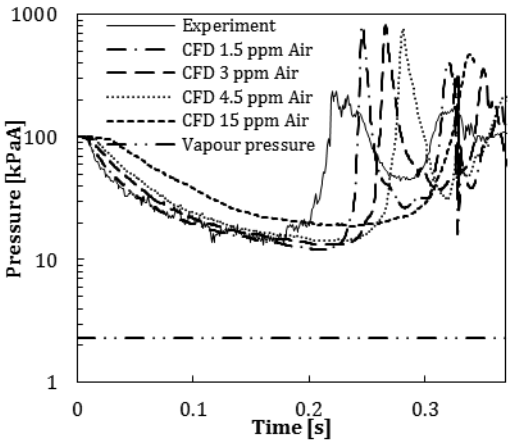

Figure 13b: Valve-seat static pressure. Experiments Vs CFD (test 3), the sensitivity to the air mass fraction is shown.

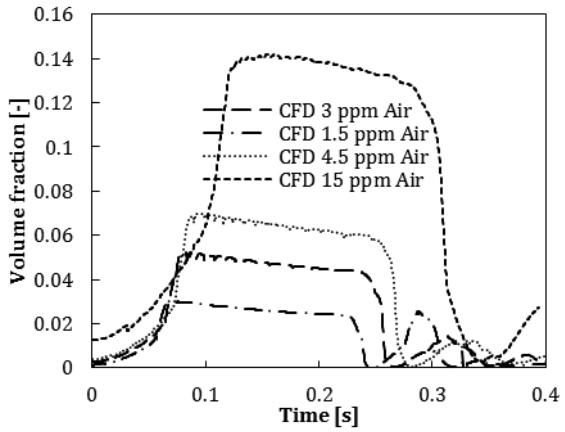

Figure 14a: The vapour volume fraction in the valve-seat lift volume according to CFD (test3).

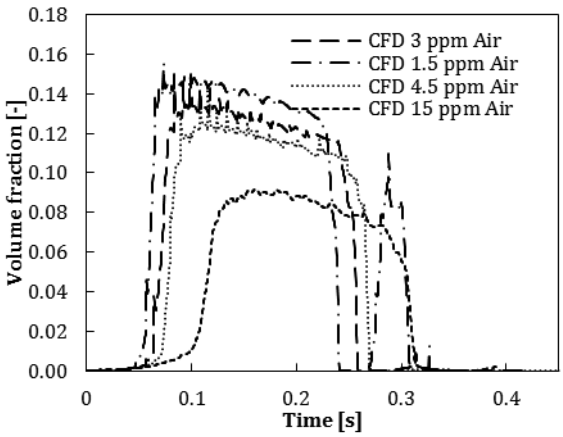

Figure 14b: The air volume fraction in the valve-seat lift volume according to CFD (test 3).

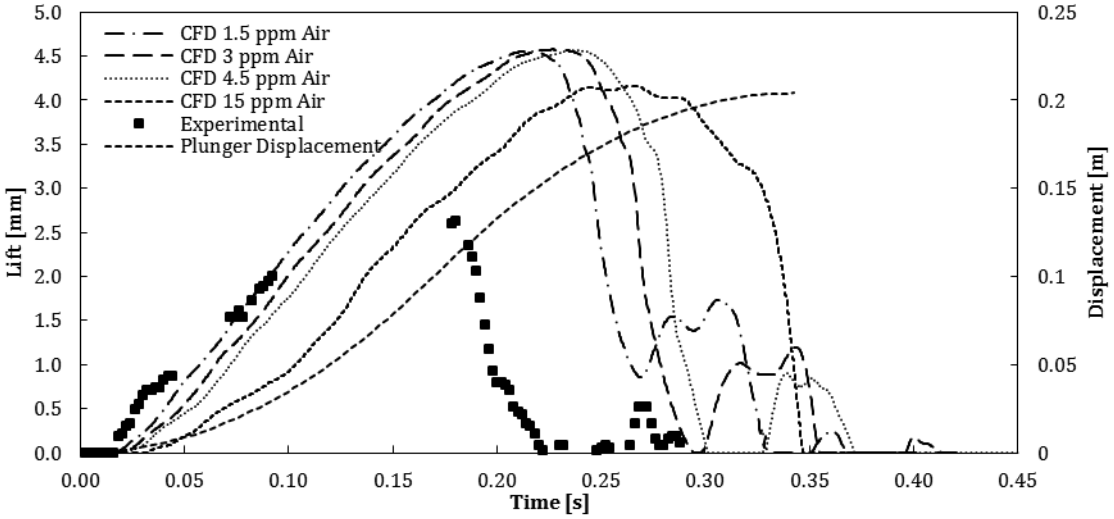

Figure 15: Test 3 valve lift, experiment Vs CFD, the sensitivity of the CFD solution to the air mass fraction is also shown.

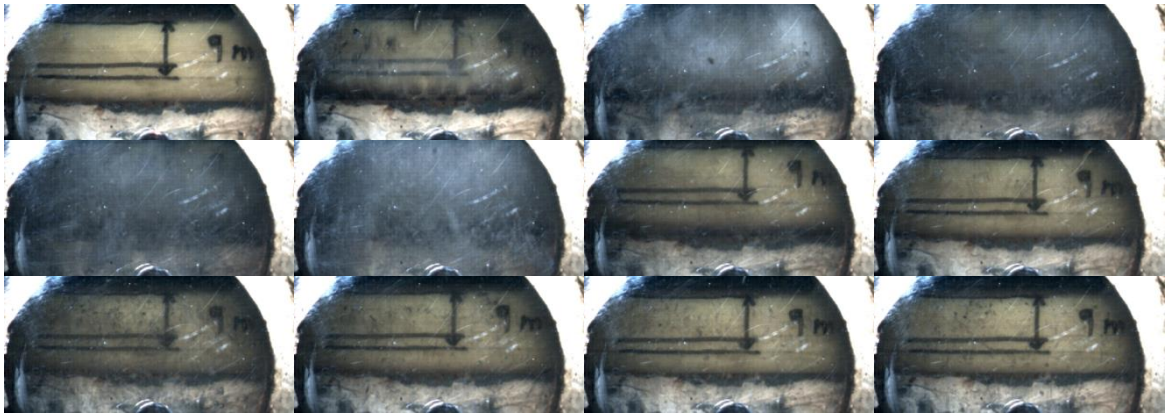

Figure 16: Full cavitation, five frames show a vapour cloud around the valve-lift gap, in four of them the view of the valve is completely obscured.

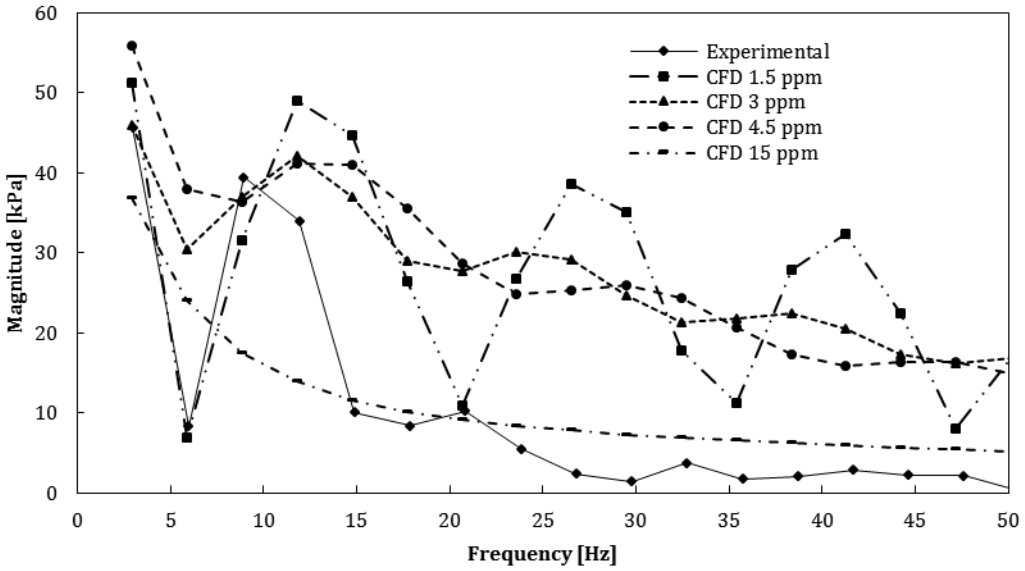

Figure 17: FFT of the chamber pressure signals, Experiment Vs CFD (test 3).